Journal of the European Ceramic Society 23 (2003) 1147–1156
www.elsevier.com/locate/jeurceramsoc

Crack deflection in piezoelectric ceramics

S.L. dos Santos e Lucato[a], H.-A. Bahr[b], V.-B. Pham[b], D.C. Lupascu[a], H. Balke[b], J. Rödel[a,*], U. Bahr[c]

[a]*Darmstadt University of Technology, Institute of Materials Science, Petersenstr. 23, 64287 Darmstadt, Germany*
[b]*Dresden University of Technology, Institute of Solid Mechanics, 01062 Dresden, Germany*
[c]*Dresden University of Technology, Institute of Theoretical Physics, 01062 Dresden, Germany*

Received 22 March 2002; received in revised form 3 July 2002; accepted 6 July 2002

Abstract

Crack deflection can occur in a specimen subject to a stress gradient of high tensile stresses near the surface which decreases with increasing depth. Such a stress gradient can be induced by strain incompatibilities. These can for example arise under electric fields between the electroded and external regions of a piezoelectric material. Such incompatibilities have been realized in thin rectangular model specimens from PZT-piezoelectric ceramics with top and bottom partial electrodes. Under an electric field, controlled crack propagation has been observed in-situ in an optical microscope. The crack paths are reproducible with very high accuracy. Small electrode widths lead to straight cracks with two transitions between stable and unstable crack growth, while large electrode widths result in curved cracks with four transitions. Poling the specimen prior to the experiment alters the crack path and introduces an anisotropy in the R-curve behavior as well as in the achievable strain mismatch. The crack path selection and crack length can be explained by means of a qualitative fracture mechanics analysis.

Keywords: Actuators; Fracture; Polarization; PZT; Toughness and toughening

1. Introduction

Crack deflection in brittle materials has been studied extensively in the past (e.g. Cook and Gordon[1] and Kendall[2]). An excellent overview of serveral loading conditions and geometries is given by Hutchinson and Suo.[3] A fracture mechanical analysis of thermal shock cracking in homogeneous materials including crack deflection has been presented by Bahr et al.[4] and He and Clegg.[5] A straight crack starting from the cooled surface in an inhomogeneous temperature and stress field will arrest at a certain depth because the crack driving force decreases with increasing depth. Yet, the crack driving force will remain constant for a crack propagating at a certain depth parallel to the surface. This can be considered as the reason for crack deflection.

One of the main difficulties in experiments under thermal loading is that the experiment cannot be stopped at an intermediate stage. This would require to maintain the temperature field inside the specimen constant. A controlled experiment with a stress gradient independent of time therefore could provide valuable mechanistic insight.

Such a loading scenario is afforded by an electric field in a partially electroded piezoelectric material. As a consequence, the ceramic material, which exhibits ferroelectric, ferroelastic as well as piezoelectric behavior, experiences a strain incompatibility between the electrically active and inactive material regions. A complex mechanical stress field arises at the electrode edge and may lead to crack initiation in this area and to crack growth.

A similar scenario is found in ceramic multilayer actuators comprised of piezoelectric materials. Investigations have revealed that cracks are formed preferentially at the internal electrode edge.[6,7] Further investigations on model and real actuators under cyclic bipolar and unipolar electric fields were performed by Schneider et al.[8,9] It was shown that cracks are formed during the first few cycles and then grow under subsequent loading. In an earlier

* Corresponding author. Tel.: +49-6151-16-6315; fax: +49-6151-16-6314.
E-mail address: roedel@ceramics.tu-darmstadt.de (J. Rödel).

0955-2219/03/$ - see front matter
PII: S0955-2219(02)00238-8

work we investigated crack initiation at the first poling cycle and could show that a large number of cracks are formed around the coercive field (E_C) and grow with increasing electric field.[10] Crack propagation as a function of the electric field in unpoled specimens has also been investigated as part of an earlier work.[11] It was shown that the crack path depends on the geometry of the specimens and the electrode. An iterative method to simulate the curved crack propagation depending on the applied electric field was proposed and predicted the experimental results with very high accuracy.

In this work we are analyzing crack growth during the first polarization or repolarization cycle in a model geometry using an electric field to introduce a strain gradient. The specimens are poled in plane to introduce an anisotropy in the elastic constants as well as in the fracture toughness. Macroscopic piezoelectricity is also introduced by poling constituting an additional complexity. Utilization of a ferroelectric material permits the investigation of piezoelectric fracture criteria which are subject to the electro-mechanical coupling.

The same specimen geometry and material of a previous investigation[11] have been chosen to compare the results. Thin rectangular specimens with partial electrodes located along the same edge of the top and bottom sides and a pre-crack were used as shown in Fig. 1. If an electric field is applied between the two electrodes the material will contract in the directions perpendicular to the field and expand in the direction of the applied electric field. It would do so freely if the material between the electrodes would not be connected to the unelectroded part as shown schematically in Fig. 1b. Since the adjacent material is not affected by the electric field it will mechanically clamp the active strip and high stresses leading to crack growth arise. In order to focus solely on crack growth, a pre-crack is artificially introduced. Please note that the deformation shown in Fig. 1b is not the true deformation and is used solely to schematically introduce the origin of the stresses.

2. Experimental methods

All experiments were performed on a commercial lead zirconate titanate, PIC 151 (PI Ceramics, Lederhose, Germany). The specimens were delivered as plates of dimensions $38\times33.5\times1$ mm^3 for the R-Curve measurements and $40\times40\times0.5$ mm^3 for all other experiments. The specimens in this work were sintered in two batches, both using powder from the same batch. All experiments with unpoled specimens consisted only of material of the first sinter batch while the second batch was used exclusively for the experiments with poled specimens. They were all polished on one side to a 1 μm finish. Due to different polishing times for the different specimens, a small variation of the final thicknesses arose.

Some of the specimens were then poled in plane (not in thickness direction) with a field of 1.5 E_C (with $E_C = 1$kV/mm this required up to 60 kV for the largest dimension). Particular care had to be taken to avoid dielectric breakdown at these high voltages. A special poling device was built using components of Fischertechnik® (Construction-set of Nylon®) and kept in a plastic bucket filled with silicone oil. Prior to poling, electrodes were silver painted onto the small sample surfaces as shown in Fig. 1d. These electrodes were carefully washed off with acetone after the poling process.

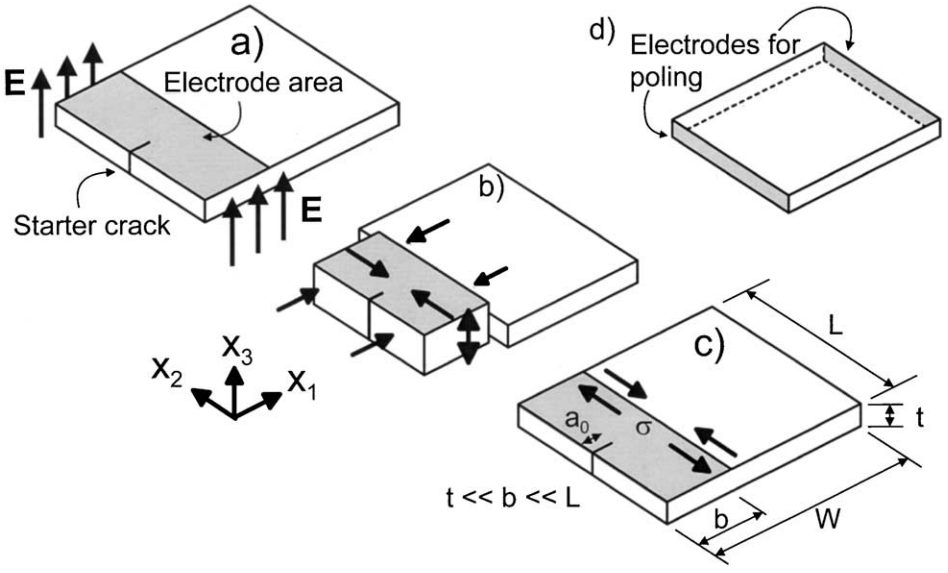

Fig. 1. Stress generation by mechanical clamping due to partial electrode coverage. (a) Electric field is applied at the electrodes (active material). (b) Shrinkage in x_1 and x_2 directions and expansion in x_3 direction of the active part would ensue if the active part would be free. (c) Adjacent material mechanically clamps the active strip and high tensile stresses arise. (d) Electrode configuration for in plane poling.

Three different experiments were performed. First, the material resistance to crack propagation was measured in the form of R-curves. In the second experiment the achievable displacement was measured. As the crack driving force depends on the achievable strain, the displacement allows a qualitative estimate of the driving forces. Finally the crack propagation driven by electrically induced strain is measured.

A coordinate system is used in all experiments as follows. Direction x_3 is the electrical field direction (thickness direction), x_2 is parallel to the electrode edge and x_1 is perpendicular thereto forming a right hand co-ordinate system (Fig. 1). The electrode coverage is defined by b/W, were b is the electrode width and W the specimen width. The volume between the electrodes will be defined as active material and the remainder inactive material. The length of the electrode is given by the length L.

2.1. R-curve measurements

The R-curves were measured in compact tension geometry. Only unelectroded specimens were used because the mechanical behavior in the inactive area is of interest for the crack deflection. Plates with 0.5 mm thickness proved too fragile for mechanical loading. Therefore, R-curves were obtained using the 1 mm thick plates cut to compact tension specimen. The test itself was performed based on ASTM 399.[12] The CT testing device is a new version of the type used before[13] and was mounted on a coordinate stage on an optical microscope. A computer with a custom designed software connected to the stage is used to read out the stage coordinates and the applied load. The crack length was obtained by targeting the crack-tip with the crosshairs in the eyepieces. With the crack-length and applied load known, the applied stress intensity factor and the crack growth velocity were calculated in real time by the data-acquisition software. The crack growth is maintained at a constant velocity throughout the whole measurement.

Prior to the R-curve measurement a sharp pre-crack was produced using a half chevron notch and a Knoop indent with a load of 50 N as described in Rödel et al.[13] After the pre-crack had been driven through the region of the half chevron notch, it was then renotched to a final length of approx. 600 μm. The end of the notch is used as origin for the crack extension Δa. To ensure maximum reproducibility, special care was taken to record data at crack velocities of about 10^{-6} m/s. A data point was recorded every 25 μm up to the final crack extension of about 5 mm. The crack propagates in the direction x_1 of the previously defined coordinate system. Unpoled specimens as well as specimens poled parallel and perpendicular to the crack propagation direction, i.e. x_1 and x_2 direction, were prepared.

2.2. Displacement measurements

Displacements were measured in x_2 direction using specimens with 0.5 mm thickness cut to 20×20 mm^2. The actual preparation procedure was as follows: First electrodes of Au/Pd (80%/20%) with a final thickness of approx. 50 nm were sputtered onto the large surfaces. Thin copper wire connections to the high voltage source were glued onto both electrodes using a conducting 2-component epoxy. Two unpoled and 4 poled specimens were prepared.

A linear variable displacement transducer (LVDT) with a very thin alumina tip was used as shown in Fig. 2. The tips of the LVDT and the ground fixture were very carefully centered on the specimen side faces. In order to prevent arcing at these high fields the specimens were placed in a cup filled with Flourinert® 77 (3M Corporation). An electric field, E_3, of up to 4 kV/mm (approx. 4 E_C) was then applied at a rate of 12.5 V/(mm/s) for the displacement measurement. The data was logged with a rate of 50 points per second. Two poled specimens were measured with the polarization in x_2 direction and two more with the polarization axis in x_1 direction. Two unpoled specimens were measured as reference.

2.3. Crack propagation measurements

The specimen preparation for the crack propagation under electric driving field was slightly different from the above described procedure. The specimen size was 40×40 mm^2 with a thickness of 0.5 mm. In the first step electrodes were sputtered onto the surfaces. To achieve only partial coverage as shown in Fig. 1 stencils of overhead transparencies were cut and attached to both surfaces by superglue and removed after sputtering. The electrodes had a final thickness of approx. 50 nm. Two

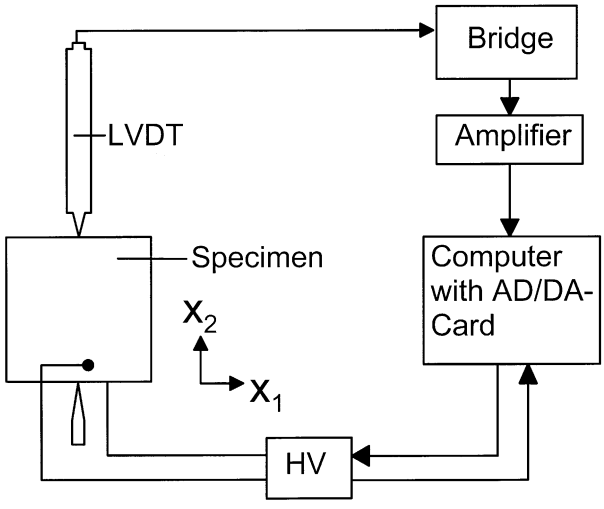

Fig. 2. Experimental set-up to measure the displacement hysteresis loop.

electrode widths were prepared in every polarization state. Electrodes of 1 and 2 mm width were prepared using unpoled plates and plates poled in x_2 direction (parallel to the electrodes). Plates poled in x_1 direction (perpendicular to the electrode) were investigated with electrodes of 2 and 3 mm width. A narrow strip of silver—paint was applied along the center of each electrode to ensure complete contact along the electrode length in all stages of cracking. Thin copper wires were glued parallel to the electrode edge on both electrodes using a conducting 2-component epoxy to connect both sides of the crack. One side of each copper wire extended beyond the specimen edge and served as connection to the high voltage source.

Finally, a precrack was introduced by placing a Knoop indent onto the front specimen face (40×0.5 mm^2). The specimen was clamped in upright position by a high-precision wrench and the indent was placed using a load between 30 and 50 N for 10 s depending on the desired crack length. The elastic–plastic contact zone with the residual stress zone was sanded away using alumina paper. A sharp precrack through the entire thickness was thus achieved.

The precracked specimens were placed in a fixture filled with Flourinert® 77 for electrical insulation. The fixture was mounted onto the coordinate stage in the optical microscope and a high-voltage source was connected to the specimen. A computer with an AD/DA-card was used to control the HV-source. In the measuring cycle the electrical field E_3 applied to the specimen was increased in steps of 68 V/mm at a ramp of 12.5 V/(mm/s). After waiting for approx. 30 s the crack-tip was targeted with the crosshairs in the eye pieces of the optical microscope and the coordinates were transferred to a custom designed CAD-type software. The waiting time was inserted to let the crack grow subcritically to a very low velocity and therefore maintain uniform conditions for all data points. The increment-measurement cycle was repeated until no further crack growth was observed.

3. Results

3.1. Measured R-curves

As the crack was not renotched to small lengths and the specimens were not thermally depolarized after growing the starter crack, the initial value of the R-curve could not be measured with high precision. The R-curves start at about 0.8–0.9 MPam$^{1/2}$ (Fig. 3). A steep rise up to 1.15 MPam$^{1/2}$ is observed in the first 500 μm of crack extension. It changes into a linear increase of the fracture toughness up to an extension of about 3.5 mm after which the fracture toughness becomes constant. These final toughness values are termed plateau values and range from 1.17 MPam$^{1/2}$ in the specimens poled in x_2 direction (perpendicular to the crack), 1.36 MPam$^{1/2}$ in specimens poled in x_1 direction (parallel to the crack), up to 1.45 MPam$^{1/2}$ in the unpoled specimens. The ranking of these results agrees well with measurements in thicker specimens.[14]

As most domains are orientated in the loading direction due to poling in the specimens poled in x_2 direction very little reinforcement can be contributed from domain switching. Some reinforcement is still possible as not all domains are aligned by poling. Theoretically the domains in the specimens poled in x_1 direction should be able to switch as they are not oriented in the direction of the principal stresses. However, due to mechanical clamping by the full sample length in the crack propagation direction, switching is limited.

The comparison between the poled and unpoled results has to be made carefully as the specimens originated from different sintering batches. The R-curves and the corresponding crack growth velocity are shown in Fig. 3. The crack growth velocity was maintained at about 10^{-6} m/s with deviations of less than a factor of 3.

3.2. Displacement measurements

The measured displacements for the different poling states are shown in Fig. 4. As the transverse displacement is measured, large displacements are more negative than small ones. Specimens poled in x_1 direction (perpendicular to the measurement axis) exhibited the smallest displacement of -35 ± 1.7 μm. Unpoled specimens show a maximum displacement of -49 ± 1.1 μm and the largest displacement of -78 ± 5.1 μm was measured in specimens poled in x_2 direction (parallel to the measurement axis). These values correspond to strains of 0.088, 0.123 and 0.195%, respectively. This is in good agreement with measurements made by Huber et al.[15]

In a simplified consideration only domains aligned parallel to the measurement direction contribute to the measured displacement. The achievable displacement therefore increases with the number of domains oriented along the measurement axis. In specimens poled in x_1 direction only very few domains remained in the direction parallel to the measurement axis during poling and do now contribute to the measured displacement. In the specimens poled in x_2 direction most domains are aligned with the measurement axis while only about 1/3 of the domains in the unpoled state are oriented in parallel direction. Therefore the displacement in the unpoled specimens should be 1/3 of the difference between the two poled directions higher than the value for the x_1 direction. This equals -49 μm, exactly the result for the unpoled specimen. The ranking in displacement is thus easily understood.

The scatter shown as thin lines in Fig. 4 is smallest for the unpoled specimens and is larger in specimens poled in x_1 and x_2 direction. The main reason for the scatter is

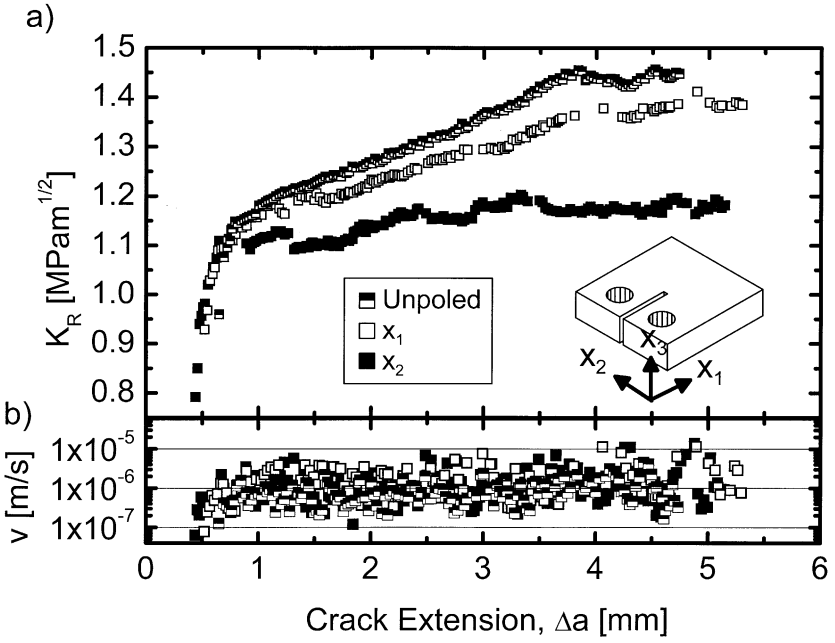

Fig. 3. (a) R-curve for unelectroded specimens poled in x_1 and x_2 direction as compared to unpoled specimens (b) Corresponding crack growth velocity.

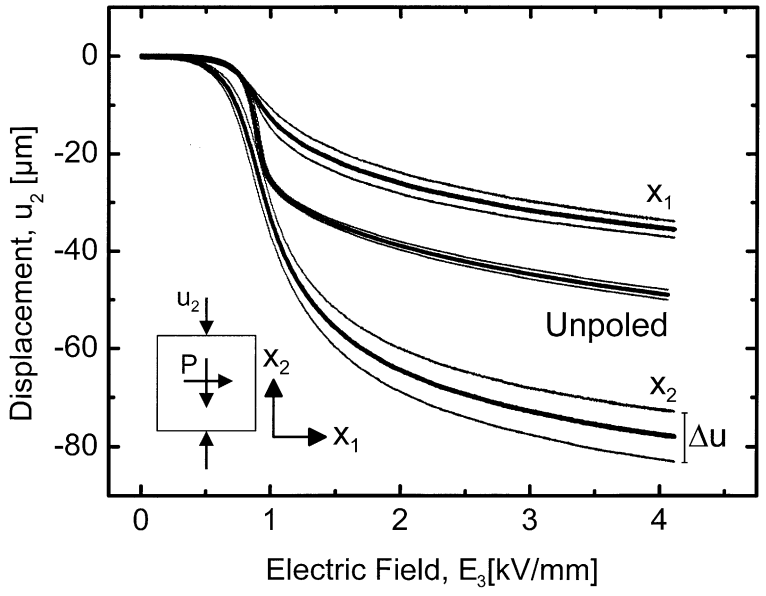

Fig. 4. Displacements in x_2 direction of poled and unpoled free specimens ($20\times20\times0.5$ mm^3). The scatter is shown as thin lines.

a misalignment of the polarization axis compared to the measurement axis. This misalignment will have a larger effect in the poled specimens as those are textured due to the poling, while the unpoled specimens are isotropic.

3.3. Crack propagation measurements

3.3.1. Unpoled specimens

Two different crack paths are observed in the unpoled specimens. In specimens with an electrode width of 1 mm a straight crack is found while in specimens with 2 mm wide electrodes the crack deflects and grows to remarkable lengths. Such a deflected crack is shown in Fig. 5a. Two experiments were done with that electrode width and the crack path could be very well reproduced as seen in Fig. 5b. The simulation of the crack progagation[11] showed that the contour of the crack is given solely by the criterion of local symmetry[16] ($K_{II}=0$, K denotes the stress intensity factor). The result of the simulation is shown as solid line in Fig. 5b.

The crack length vs. electric field data were evaluated from the above measurements and are shown in Fig. 6

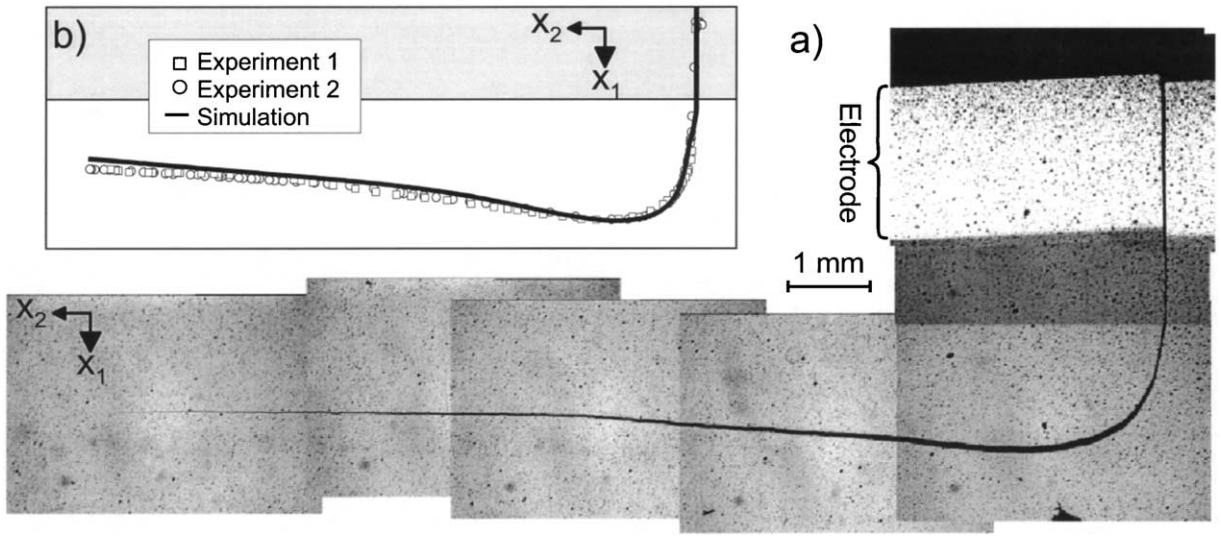

Fig. 5. (a) Photograph of final crack configuration for a curved crack in an unpoled specimen (b) Comparison of two different experiments and the simulation.[11]

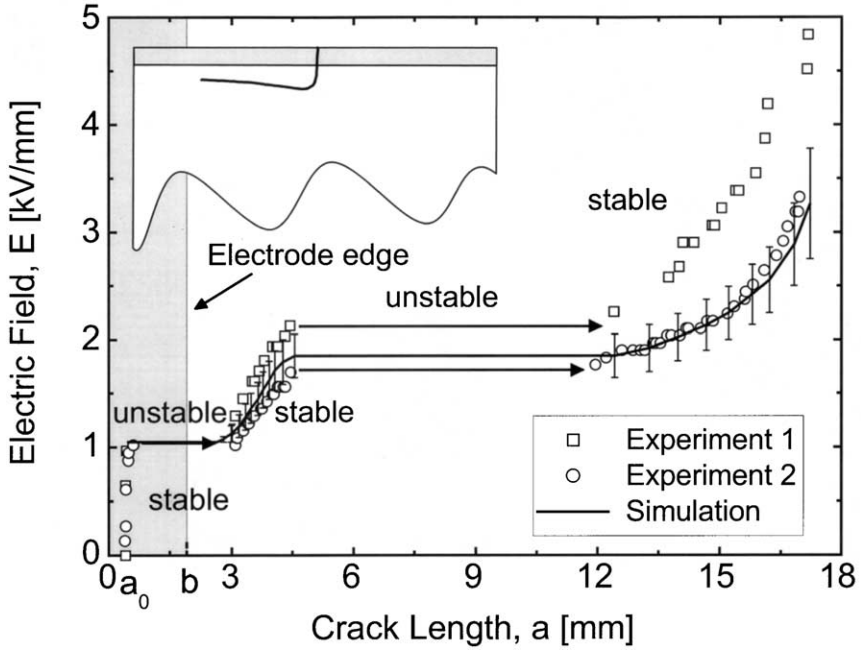

Fig. 6. Measured crack length as a function of the electrical field for the unpoled specimen with $b = 2$ mm. Note the four transitions between stable and unstable crack propagation. The crack path as observed in the optical microscope is shown in the insert.

along with the result of the simulation.[11] Two regions of unstable and 3 regions of stable crack growth are observed. Crack propagation started at an initial crack length of approx. 0.5 mm and continued stable up to a length of approx. 0.6 mm corresponding to an electric field of about 1 kV/mm. At this point the crack grew unstable beyond the electrode edge to a final length of about 3 mm. A second region of stable crack growth followed up to a length of approx. 4.5 mm. The crack deflection is located in this region and a second unstable crack growth region followed after the deflection with the crack now growing nearly parallel to the electrode edge. This second unstable stage extended over approx. 7.5 mm. Finally the crack grew stable to the final length of about 16.5 mm.

The results of both experiments are shown in Fig. 6. While the stable/unstable transition crack lengths are well reproducible, the electric fields are not. The difference between the two experiments increases with increasing crack length. The result of the simulation is also shown with error bars resulting from the displacement measurements, which served as input data into the

simulation. Since the displacements and the R-curves were the only experimental inputs into the simulation, it can be concluded that the difference between the two experiments can be mainly attributed to the scatter in the displacements and therefore to the crack driving force as well as to the scatter in the R-curves.

3.3.2. Poled specimens

In the next step the specimens were poled along one of the long axes of the specimen (x_1 or x_2 direction) and the experiments were repeated. An overview over all investigated electrode widths and polarization states is provided in Fig. 7a. The two possible crack paths, straight and deflected, are also observed in the poled specimens but with different electrode widths. Only deflected cracks are observed in specimens poled in x_2 direction (parallel to the electrode) even with an electrode width of 1 mm where the crack is straight in an unpoled specimen. In specimens poled in x_1 direction (perpendicular to the electrode) only straight cracks are observed up to an electrode width of 3 mm. Common to all experiments was that the direction of the deflection was not correlated to the poling direction regardless of the polarization state.

Increasing electrode width in the specimens poled in x_2 direction (middle row in Fig. 7a) results in increasing lengths of the unstable regions as well as increasing deflection depths, i.e. the distance form the specimen edge. The first unstable region in specimens with an electrode width of 1 mm extends from 0.5 to 1.4 mm and from 0.6 to 2.6 mm for a 2 mm electrode. An extension of the second unstable region from 2.5 to 4 mm and from 6.6 to 11.9 mm is observed for 1 and 2 mm electrode widths, respectively. The final deflection depth is 2.9 mm (1 mm electrode) and 3.7 mm (2 mm electrode).

Comparison of the various electrode widths in the x_1 polarization direction (lower row in Fig. 7a) reveals an increase in the stable/unstable transition crack lengths as well as the final crack length with increasing electrode width. The start and end of the unstable region was at a crack length of 0.8 mm/2.7 mm in the 2 mm electrode and 0.9 mm/3.6 mm in the 3 mm electrode. Yet, the transition electric field remained almost constant at 1.4 kV/mm. As all the cracks remained straight only one unstable region is observed.

The remainder of this work will be focused on an electrode width of 2 mm in unpoled specimens and specimens poled in x_2 direction. In both cases the crack path is very well reproducible (Fig. 7b). Yet, the crack path itself differs slightly between the two polarization cases (Fig. 8). While the crack turns by almost exactly 90° in the poled case and continues to grow parallel to the electrode edge, it turns by approx. 98° in the unpoled case and the distance to the specimen edge decreases with further crack growth. Furthermore, the first straight section of the crack is longer in the unpoled case than in the parallel poled case.

Finally the crack length as a function of the applied electric field can be compared between the two polarization states as it is done in Fig. 9. Two major differences can be observed. First, the electric field required to drive the crack to a certain length is significantly lower in the specimens poled in x_2 direction than in the unpoled specimens. Second, in the poled specimens the crack does not "pop" through the second "unstable" region to the final length, but it grows at a velocity such that the experiment can still be followed in the optical microscope.

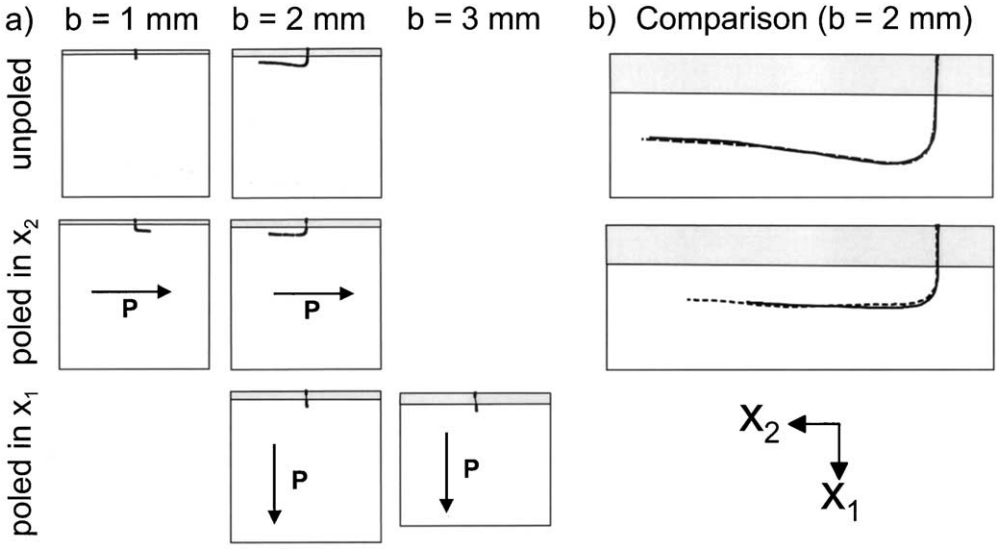

Fig. 7. (a) Overview of the crack paths in the investigated geometries (b) Comparison of the crack path for specimens with an electrode width of 2 mm. The different experiments are marked by different type line.

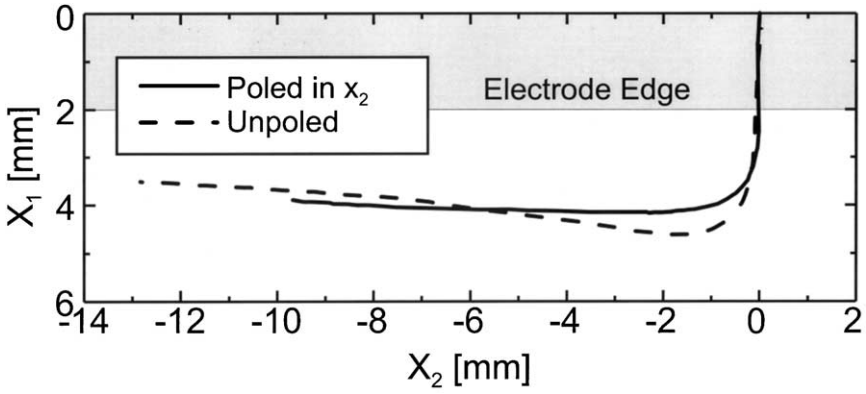

Fig. 8. Comparison of the crack path in unpoled specimens and specimens poled in x_2 direction.

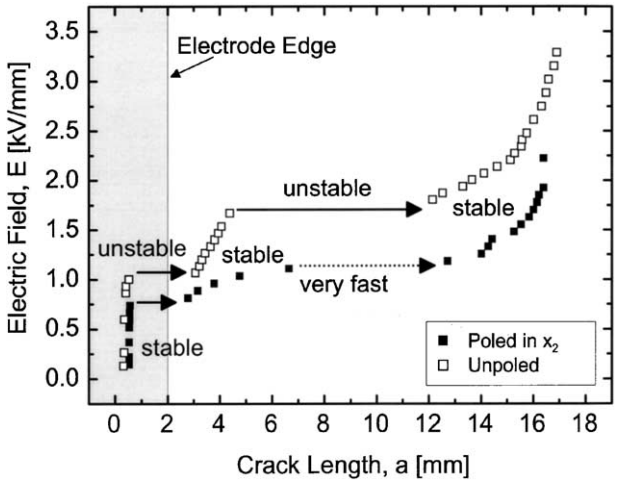

Fig. 9. Comparison of the crack length as a function of the electric field between specimens with an electrode width of 2 mm in unpoled specimens and specimens poled in x_2 direction.

4. Discussion

For a qualitative discussion of the observed experimental results we use an energy release rate based crack propagation criterion for an anisotropic piezoelectric material. Accordingly, a crack grows in the direction of maximum energy release rate ratio:

$$\frac{G(\theta)}{G_C(\theta)} \rightarrow \text{Max.} \tag{1}$$

G and G_C are the energy release rate and the critical energy release rate, respectively. They are functions of the direction angle θ to the pre-existing crack. The crack propagates in this direction if the fracture condition

$$G(\theta) \geqslant G_c(\theta) \tag{2}$$

is fulfilled. For the isotropic case as in the unpoled specimens (1) is equivalent to the criterion of local symmetry[14] ($K_{II}=0$) and (2) becomes $K_I \geqslant K_{Ic}$, where K_{Ic} is the critical stress intensity factor or the fracture toughness. G_C can be determined from the measured plateau values of the R-curves (Fig. 3).

In a first strictly qualitative approximation the investigated specimens can be treated as a semi-infinite medium loaded with a stress σ along an edge strip of width b corresponding to the electrode area. A straight crack far way from the active area behaves like an edge crack under point load at the crack mouth and $G \sim \sigma^2 b^2/a$ decreases with increasing a. The energy release rate of a primary straight and then deflected crack (delaminated crack) is

$$G = \alpha \sigma^2 b / Y_{22} \tag{3}$$

with Y_{22} as the Young's modulus of the inactive material in x_2-direction and α as a function of the elastic mismatch between the active and the inactive zone. The dielectric displacement intensity factor due to piezoelectric coupling is not taken into account. The delamination depth d, which is the distance from the specimen edge to the crack running parallel to the edge after it has deflected, results from the condition (1).

While the asymptote for $a \rightarrow \infty$ for the straight crack is $G=0$, it is $G>0$ ($G=0.343\ \sigma^2 b/Y$ in the isotropic case[3]) for the deflected crack. Consequently the straight crack will always arrest at a certain length as soon as (2) ceases to be valid. Another consequence is that the energy release rate of the deflected crack path in the inactive area at a given crack length is always higher than for the straight crack. According to (1), it can be concluded that in all the investigated geometries a primary straight crack is prone to deflect. In fact, the crack deflects even in specimens poled in x_2 where G_C in x_2-direction is higher than in x_1 (Fig. 3). It is interesting to note that in some situations the crack seems to prefer to propagate in the direction with the higher G_C. However, the crack driving force G in this direction is much higher than in other directions, such that the ratio G/G_C is maximal in this direction.

The observed crack paths in Fig. 7 can be explained in a simplified treatment: As discussed above the crack

chooses a deflected path on which it can release most energy. The attained crack length on this path depends on the material resistance G_C and on the driving force G according to (3) which is proportional to σ^2 and b. Consequently, the achieved crack length increases with wider electrodes if the stress i.e. the strain is kept constant. This is observed in each row of Fig. 7a. If the attained crack length is too small as in the unpoled specimens with $b=1$ mm and in the specimens poled in x_1, θ is very small along the entire path and thus the deviation between the deflected path and the straight path is negligible and both paths are indistinguishable in the optical microscope. Therefore only the attained crack length determines whether a deflected path is observed in the experiments or if the crack remains "straight".

The influence of the polarization state is discussed for constant electrode width b corresponding to the columns in Fig. 7a. As aforementioned the obtained crack length also depends on the stress σ, which is proportional to the measured displacements. A comparison of the displacements as a function of electric field (Fig. 4) shows that the induced stress and thus the attained crack length in specimens poled in x_2 direction is the largest and in specimens poled in x_1 direction the smallest. A second consequence of the high achievable stress in specimens poled in x_2 is that, compared to an unpoled specimen, a significantly lower electric field is required to obtain the same stress and therefore crack length (Fig. 9).

According to Hutchinson and Suo[3] the delamination depth in a linear elastic orthotropic case is governed by the elastic mismatch between the active and the inactive material. Increasing stiffness of the inactive part leads to a smaller depth, if the properties of the active strip remain constant. In these experiments the active strip is always poled in x_3 direction once the crack has attained a length critical for deflection. The properties can therefore be assumed to remain the same in all specimens, while they vary in the inactive part according to the polarization state of the specimen. In a poled specimen the modulus parallel to the electrode edge is the critical one. It is 68.0 GPa in an unpoled specimen and 83.3 GPa in specimens poled in x_2 direction.[17] Accordingly, the delamination depth of the poled specimens should be smaller than that of the unpoled specimens, which is only observed for the first 6 mm after deflection (Fig. 8). First modeling results for the poled specimens indicate that the anisotropy and the influence of the piezoelectric coupling in a poled specimen which is not present in an unpoled specimen is responsible for this behavior. Additionally the investigated specimens are finite and therefore edge effects have to be considered.

Utilization of a ferroelectric material to provide the electrical field generated strain incompatibility also generates some complications. By careful choice of specimen dimensions and measurement procedure the observed complicating issues could be reduced to small effects.

The non-homogeneous electric field at the electrode edge is problematic in two ways. An electric field singularity is located underneath the electrode edge which due to the piezoelectric coupling and ferroelectric switching gives rise to locally increased tensile stresses and leads to the formation of secondary cracks along the electrode edge.[11] These cracks observed at higher electric fields can relieve the stresses at the main crack which then requires higher strains and higher electric fields for crack propagation. The density of secondary cracks is strongly reduced, if the thinnest feasible specimens are selected. A thickness of 0.5 mm proved to be the best compromise between low thickness and high survival rate during preparation. Furthermore, the electric field incorporates a fringing field next to the electrode edge, providing a volume between active and inactive material with ill-defined material properties and a highly non-homogenous stress field due to the electromechanical coupling in ferroelectrics.

A slight drawback with the choice of 0.5 mm thick plates lies in the fact, that in this thickness regime the R-curve varies with specimen thickness. The ferroelastic toughening depends on the macroscopic stress state (plane stress or plane strain) and the R-curve therefore depends on specimen thickness. Measuring the R-curve with plates of 1 mm thickness which is the thinnest possible for mechanical loading in our equipment, proved to be the best possible compromise. The thickness dependence of the R-curve may contribute to the experimental scatter in the electric field in Fig. 6.

This discussion is strictly qualitative. A quantitative discussion of the crack propagation in poled specimens requires a more detailed investigation of the involved phenomena. The simulation efforts based on (1) and (2) are ongoing and the results will be subject of a forthcoming publication.

5. Conclusion

Electrically driven crack propagation in unpoled and poled PZT ceramics has been observed. The crack path and crack length as a function of the electric field depend on the electrode geometry as well as on the poling state. The crack path selection can be discussed by means of fracture mechanics and represents a sensible indicator for suitability of a piezoelectric fracture criterion. In a first approximation the crack driving force outside the electrode edge depends on the stress in the electrode area and the electrode width. The stress is again linearly dependent on the electrically induced strain in the electrode area. As specimens poled in the x_2 direction exhibit the largest strain, a deflected crack with a large length is already achieved with narrower

electrodes. On the other hand the crack arrests at a small length in specimens poled in x_1 direction because the crack driving force is too low.

The crack path is relatively independent of small geometrical variations introduced by the manual preparation procedure. Yet, the electric field required for a certain crack length and therefore the crack driving force is highly sensitive to such variations. Differences in the deflected crack path between the unpoled and poled specimens are attributed to the material anisotropy and the piezoelectric effect not present in the unpoled specimens.

Acknowledgements

The authors gratefully acknowledge the support of this work by the Deutsche Forschungsgemeinschaft (DFG) under contract No. Rö 954/13 and Ba 1561/3. We would like to thank Thorsten Fugel from the Institut für Hochspannungstechnik, Darmstadt University of Technology for his help with the high voltage source.

References

1. Cook, J. and Gordon, J. E., A mechanism for the control of crack propagation in all-brittle systems. *Proc. R. Soc. Lond. A*, 1964, **282**, 508–5202.
2. Kendall, K., Transition between cohesive and interfacial failure in a laminate. *Proc. R. Soc. Lond. A*, 1975, **344**, 287–302.
3. Hutchinson, J. W. and Suo, Z., Mixed mode cracking in layered materials. *Adv. Appl. Mech*, 1991, **29**, 63–191.
4. Bahr, H.-A., Bahr, U., Gerbatsch, A., Pflugbeil, I., Vojta, A. and Weiss, H.-J., Fracture mechanical analysis of morphological transitions in thermal shock cracking, 6th int. symp. on fracture mechanics of ceramics, Ksarlsruhe. In *Fracture Mechanics of Ceramics, Vol. 11*, ed. R. C. Bradt et al. Plenum Publ Corp, New York, 1996, pp. 507–522.
5. He, P. and Clegg, W. J., Modeling of thermal shock spalling crack in a ceramic slab. *Key Engineering Materials*, 2000, **Vols. 183–187**, 1213–1218.
6. Aburatani, H., Harada, S., Uchino, K., Furuta, A. and Fuda, Y., Destruction mechanisms in ceramic multilayer actuators. *Jpn. J. Appl. Phys*, 1994, **33**, 3091–3094.
7. Furuta, A. and Uchino, K., Dynamic observation of crack propagation in piezoelectric multilayer actuators. *J. Am. Cer. Soc.*, 1993, **76**, 1615–1617.
8. Schneider, G. A., Rostek, A., Zickgraf, B. and Aldinger, F., Crack growth in ferroelectric ceramics under mechanical and electrical loading. In *Electroceramics IV*, *Augustinus Buchhandlung, Aachen*, edn. 1. 1995, pp. 1211—1216.
9. Schneider, G. A., Weitzing, H. and Zickgraf, B., Crack growth in ferroelectric ceramics and actuators under mechanical and electrical loading. *Frac. Mech. Cer*, 1996, **12**, 149–160.
10. dos Santos e Lucato, S. L., Lupascu, D. C., Kamlah, M., Rödel, J. and Lynch, C. S., Constraint-induced crack initiation at electrode edges in piezoelectric ceramics. *Acta Mater.*, 2001, **49**, 2751–2759.
11. dos Santos e Lucato, S. L., Bahr, H.-A., Pham, V. B., Lupascu, D. C., Balke, H., Rödel, J. and Bahr, U. Electrically driven cracks in PZT: experiments and fracture mechanics analysis. *J. Mech. Phys. Solids* (in press).
12. Standard test method for plane-strain fracture toughness of metallic materials, E399-90. *Annual Book of ASTM standards* 3.03, 1996, 407–437.
13. Rödel, J., Kelly, J. F. and Lawn, B. R., In-situ measurement of bridged crack interfaces in the scanning electron microscope. *J. Am. Ceram. Soc.*, 1990, **73**, 3313–3318.
14. dos Santos e Lucato, S. L., Lupascu, D. C. and Rödel, J., Effect of poling direction on R-curve behavior in lead zirconate titanate. *J. Am. Ceram. Soc.*, 2000, **83**, 424–426.
15. Huber, J. E. and Fleck, N. A., Multi-axial electrical switching on a ferroelectric: theory versus experiment. *J. Mech. Phys. Solids*, 2001, **49**, 785–811.
16. Cotterell, B. and Rice, J. R., Slightly curved or kinked cracks. *Int. J. Fracture*, 1980, **16**, 155–169.
17. Fett, T. and Munz, D., Measurement of Young's moduli for lead zirconate titanate (PZT) ceramics. *J. Test. Eval*, 2000, **28**, 27–35.